Supporting Information for "Retention and Transport of Silver Nanoparticles in a Ceramic Porous Medium Use for Point-of-use Water Treatment" by Dianjun Ren and James A. Smith

This Supporting Information section has 9 pages, 5 figures, and 3 tables.

Simulation of tracer and silver nanoparticle transport. The hydraulic conductivity (K) and coefficient of hydrodynamic dispersion (D) for each ceramic disk was determined by studying the transport of a conservative tracer through the porous media. Tracer experiments were conducted by using a pulse injection of tritiated water ([^{3}H]-H_2O), into the ceramic disk and sequential sampling of the effluent. The concentrations of the conservative tracer in effluent samples were quantified with a Packard 1900CA Liquid Scintillation Analyzer.

Effluent tracer and silver concentrations were simulated for parameter identification using the following one-dimensional form of the advection-dispersion-reaction equation as described previously [1-3] with the commercial software model Hydrus-1D:

$$\frac{dC}{dt} + \frac{\rho_b}{\theta_w}\left(\frac{dS_1}{dt} + \frac{dS_2}{dt}\right) = D\frac{\partial^2 C}{\partial x^2} - v\frac{dC}{dx} \quad (1)$$

$$\frac{\rho_b}{\theta_w}\frac{dS_1}{dt} = k_{att1}C - k_{\det}\rho_b S_1 \quad (2)$$

$$\frac{\rho_b}{\theta_w}\frac{dS_2}{dt} = k_{att2}C \quad (3)$$

where C is the tracer or Ag-NP concentration (ML^{-3}), ρ_b is the ceramic media bulk density (ML^{-3}), θ_w is the dimensionless volumetric water content, t is time (T), v is the linear water velocity (LT^{-1}), S_1 and S_2 are the concentrations of the Ag-NPs associated with the ceramic (solid) phase (MM^{-1}) for kinetic sites 1 and 2, respectively, D is the coefficient of hydrodynamic dispersion (L^2T^{-1}), x is longitudinal distance (L), k_{att1} and K_{aat2} are the Ag-NP attachment coefficients for kinetic sites 1 and 2, respectively, and k_{det} is the Ag-NP detachment coefficient.

Equation (1) with S=0 was used to simulate the tracer transport using D and v as fitting parameters. Then, Ag-NP transport was simulated with equations (1-3) using k_{att1}, k_{att2}, and k_{det} as fitting parameters along with the previously determined values of D and v. This model assumes that transfer of Ag-NPs from water to the ceramic matrix is kinetic and can be approximated by two first-order attachment rate coefficients and one detachment rate coefficient. The values of these parameters for all experiments that had Ag-NPs in the inflow solution are summarized in Table S1. In general, the model was able to reasonably simulate the observed effluent silver concentrations as shown in Figures 1-3 and S1.

For experiments wherein the Ag was incorporated into the ceramic disks during fabrication, the inflow solution did not contain any Ag-NPs and the release of Ag^0 from the disks

into solution was monitored over time. These data were fit to the following simple first-order model:

$$C = C_0 e^{-kt} \quad (4)$$

Table S1. Summary of experimental conditions, percentage of influent silver retained, and simulation parameters for silver-nanoparticle transport experiments through ceramic disk with nanoparticles present in the inflow solution to the ceramic porous media.

No.	Silver nanoparticle	Ionic strength cm/min	Flow rate mL/min	Percent silver retained	Rate coefficient, min^{-1}		
					k_{att1}	k_{det}	k_{att2}
1	Argenol	1	0.6	16	0.141	0.236	0.015
2	Argenol	10	0.6	27	0.220	0.239	0.023
3	Argenol	50	0.6	71	0.461	1.240	0.085
4	NanoXact-10	1	0.6	20	0.053	0.065	0.017
5	NanoXact-10	10	0.6	45	0.035	0.017	0.032
6	NanoXact-10	50	0.6	59	0.079	0.563	0.099
7	NanoXact-50	1	0.6	21	0.172	0.340	0.018
8	NanoXact-50	10	0.6	49	0.277	0.842	0.038
9	NanoXact-50	50	0.6	76	2.615	6.613	0.069
10	NanoXact-100	1	0.6	16	0.089	0.094	0.013
11	NanoXact-100	10	0.6	70	0.290	0.453	0.080
12	NanoXact-100	50	0.6	100	-	-	-
13	NanoXact-50	1	3	13	1.317	2.352	0.048
14	NanoXact-50	1	0.2	30	0.052	0.031	0.008

where C_0 is the initial effluent concentration measured in the experiment (ML^{-3}) and k is a first-order rate coefficient (T^{-1}). Parameter values for the experiments shown in Figures 5 and 7 are summarized below in Table S2.

Table S2. Initial effluent silver nanoparticle concentrations, C_0, and first-order rate coefficients for the model fits to the experimental data depicted in Figures 5 and 7 for different flow rates and solution ionic strengths.

		Dipping		Paint-on	
		C_0, mg/L	k, min^{-1}	C_0, mg/L	k, min^{-1}
Flow Rate (mL/min)	0.6	13.2	-0.0174	14.8	-0.0202
	1.2	1200	-0.0335	690	-0.0329
Ionic Strength (mM)	11	2.54	-0.0198	1.33	-0.0138
	0	3.49	-0.0142	1.08	-0.00868

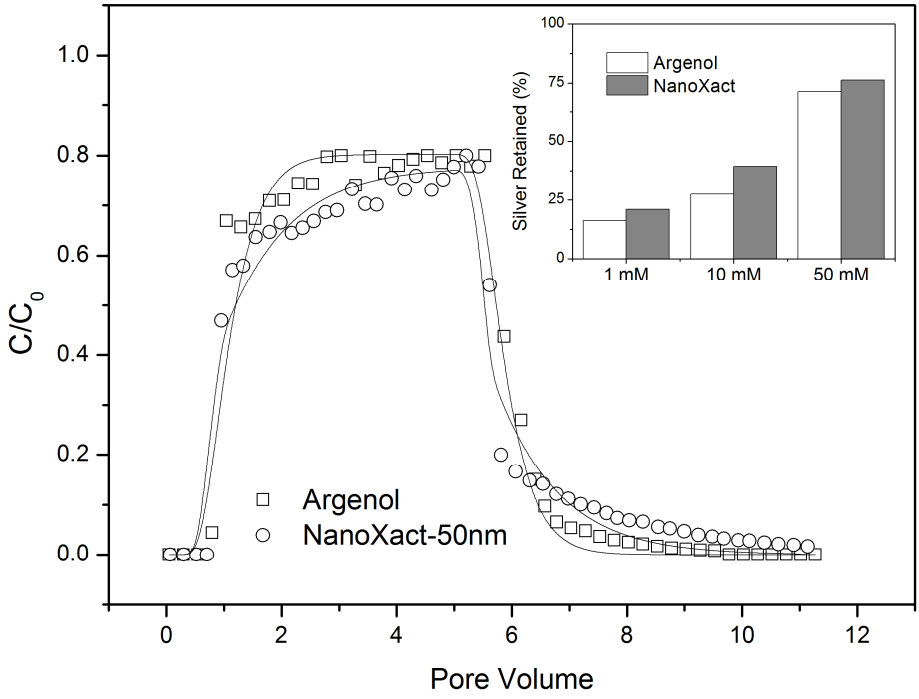

Figure S1. Plots of effluent total silver concentration from ceramic disks (C) normalized to the influent total silver concentration (C_0) as a function of pore volumes of flow for Argenol silver proteinate and NanoXact 50-nm nanoparticles at a solution ionic strength of 1 mM and a flow rate of 0.6 mL/min. Inset: Percent silver retained in the ceramic disk at each ionic strength (1 mM, 10 mM, and 50 mM) and for both types of silver nanoparticles.

Ceramic/Ag-NP Interaction Energies. Classical DLVO theory can be modified to account for AgNP interaction with ceramic surfaces. As mentioned in the main text, the combined attractive force, Φ_T, between the Ag-NP and the ceramic surface is the summation of the van der Waals (vdW) attraction and electrostatic double layer repulsion (EDL) as shown below:

$$\Phi_T(h) = \Phi_{SwS}^{vdW}(h) + \Phi_{SwS}^{EDL}(h) \tag{5}$$

This combined force determines the stability of nanoparticles in the aqueous phase. In this study, we simplified the interaction between nanoparticle and ceramic surface to that between nanoparticle and an infinite flat surface. The attraction from van der Waals forces, Φ_{SwS}^{vdW}, is expressed as [4]:

$$\Phi_{SwS}^{vdW}(h) = -\frac{A_{123}}{6}\left[\frac{a}{h} + \frac{a}{h+2a} + \ln\left(\frac{a}{h+2a}\right)\right] \quad (6)$$

where, h is the separation distance and a is the particle radius ($d_p/2$). A_{123} refers to the overall Hamaker interaction constant for the deposition of nanoparticle "1" onto a surface of collector "3" when suspended in the medium of water "2". The individual Hamaker constants for mediums 1, 2, and 3 in a vacuum are denoted as A_{11}, A_{22}, and A_{33} (Table S3) and are used to calculate A_{123} through the following relation:

$$A_{123} = (A_{33}^{0.5} - A_{22}^{0.5})(A_{11}^{0.5} - A_{22}^{0.5}) \quad (7)$$

Repulsion from the electrostatic double layer is given as [5, 6]:

$$\Phi_{SwS}^{EDL}(h) = 64\pi\varepsilon_0\varepsilon_r a\left(\frac{k_B T}{ze}\right)^2 \Gamma_1\Gamma_2 e^{-\kappa h} \quad (8)$$

where, ε_0 is vacuum permittivity, ε_r is the dielectric constant of the medium (in this case, water), z is the valence of electrolyte, e is electron charge, k_B is the Boltzmann's constant, Γ_1 and Γ_2 are the surface potentials for the AgNP and sand surfaces, respectively, and κ is the reciprocal of the Debye length. The inverse of the Debye length is given as follows:

$$\kappa^{-1} = \sqrt{\frac{\varepsilon\varepsilon_0 k_B T}{2000 N_A I e^2}} \quad (9)$$

where N_A is Avogadro's number and I is the ionic strength.

Table S3. Hamaker constant for silver nanoparticles, water and ceramic disk

Material	Hamaker Constant (10^{-20} J)	Reference
Silver Nanoparticles	38.5	[11, 12]
Water	3.7	[10]
Ceramic (derived from clay)	4.89	[7-9]

Figures S2-S5 present the calculated interaction energies between each type of Ag-NP as a function of separation distance at each solution ionic strength.

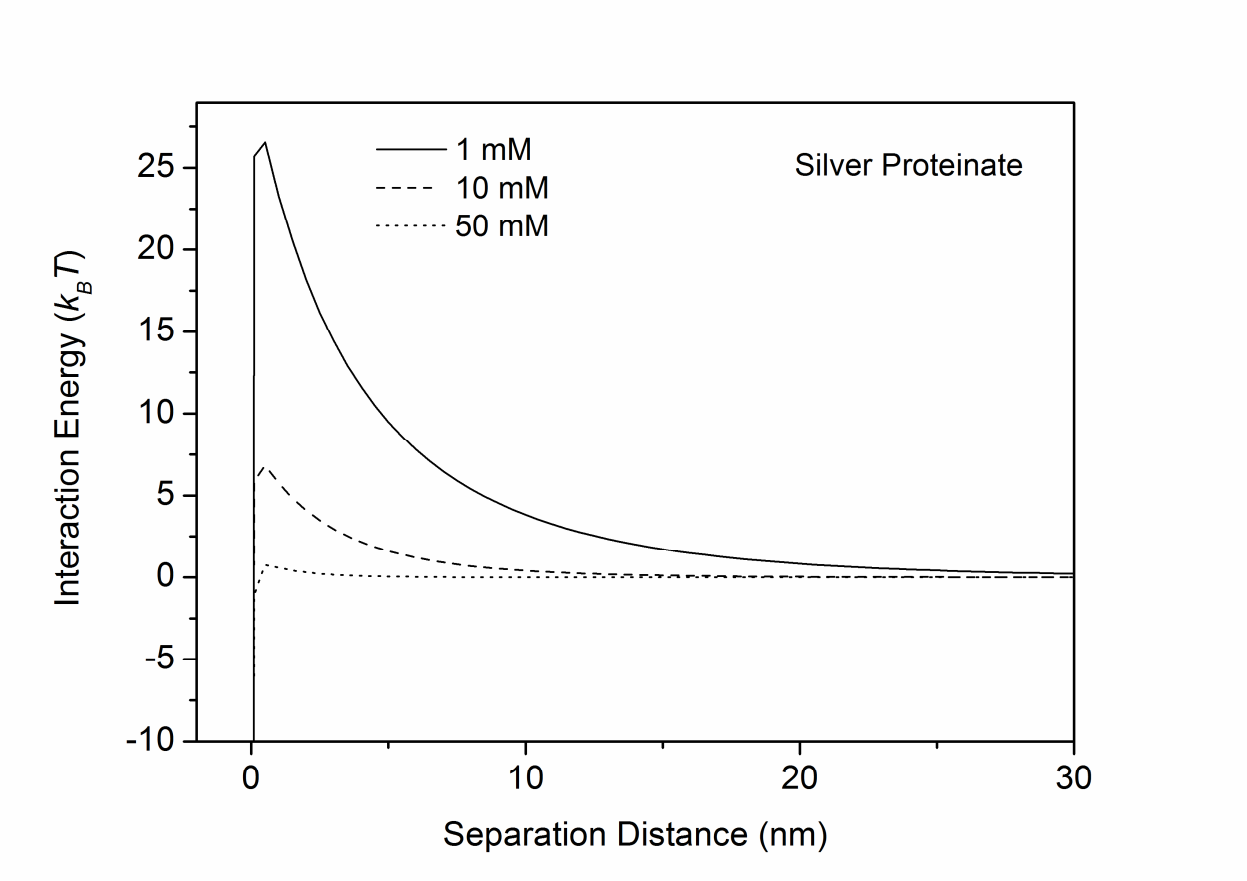

Figure S2. Interaction energy profile between silver proteinate nanoparticles and the ceramic collector surface as a function of separation distance for three ionic strengths.

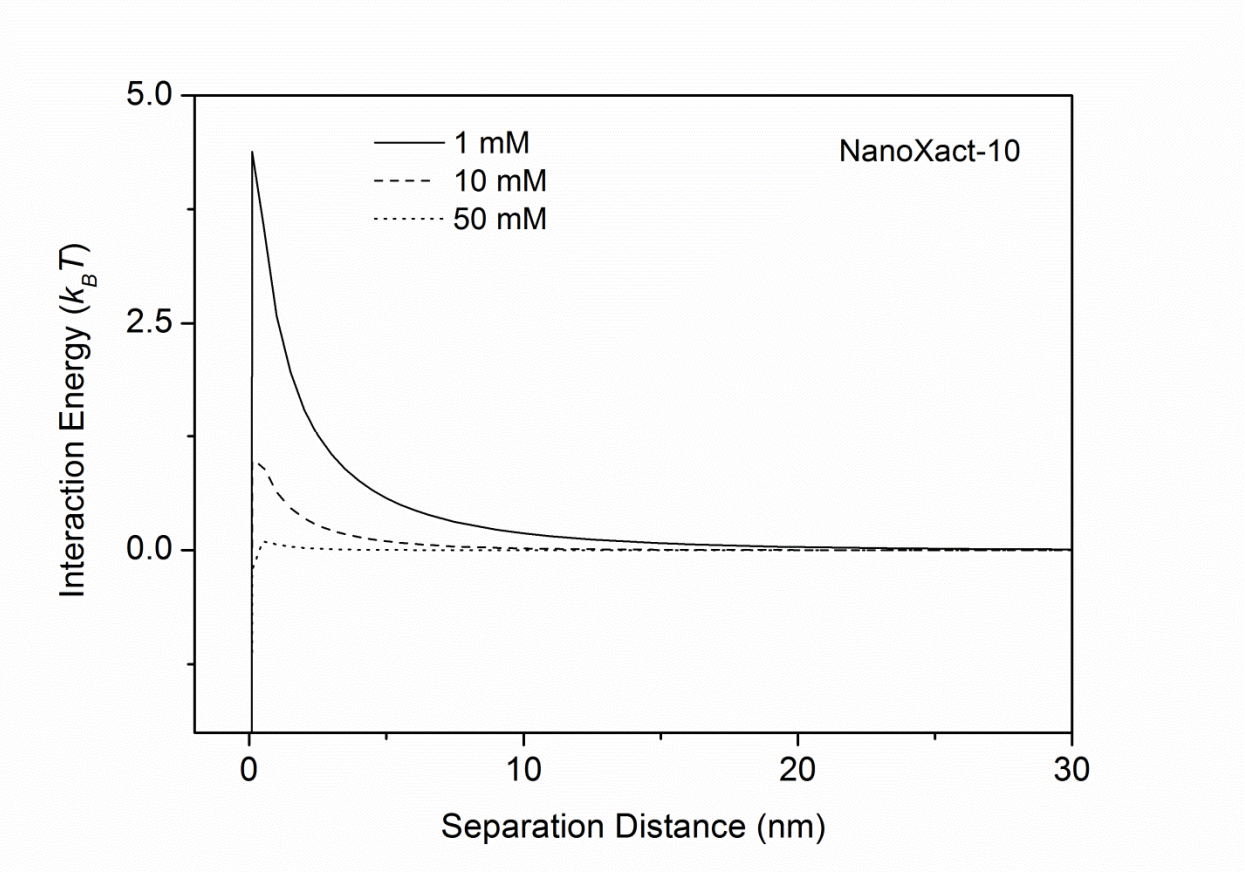

Figure S3. Interaction energy profile between NanoXact-10 nanoparticles and the ceramic collector surface as a function of separation distance for three ionic strengths.

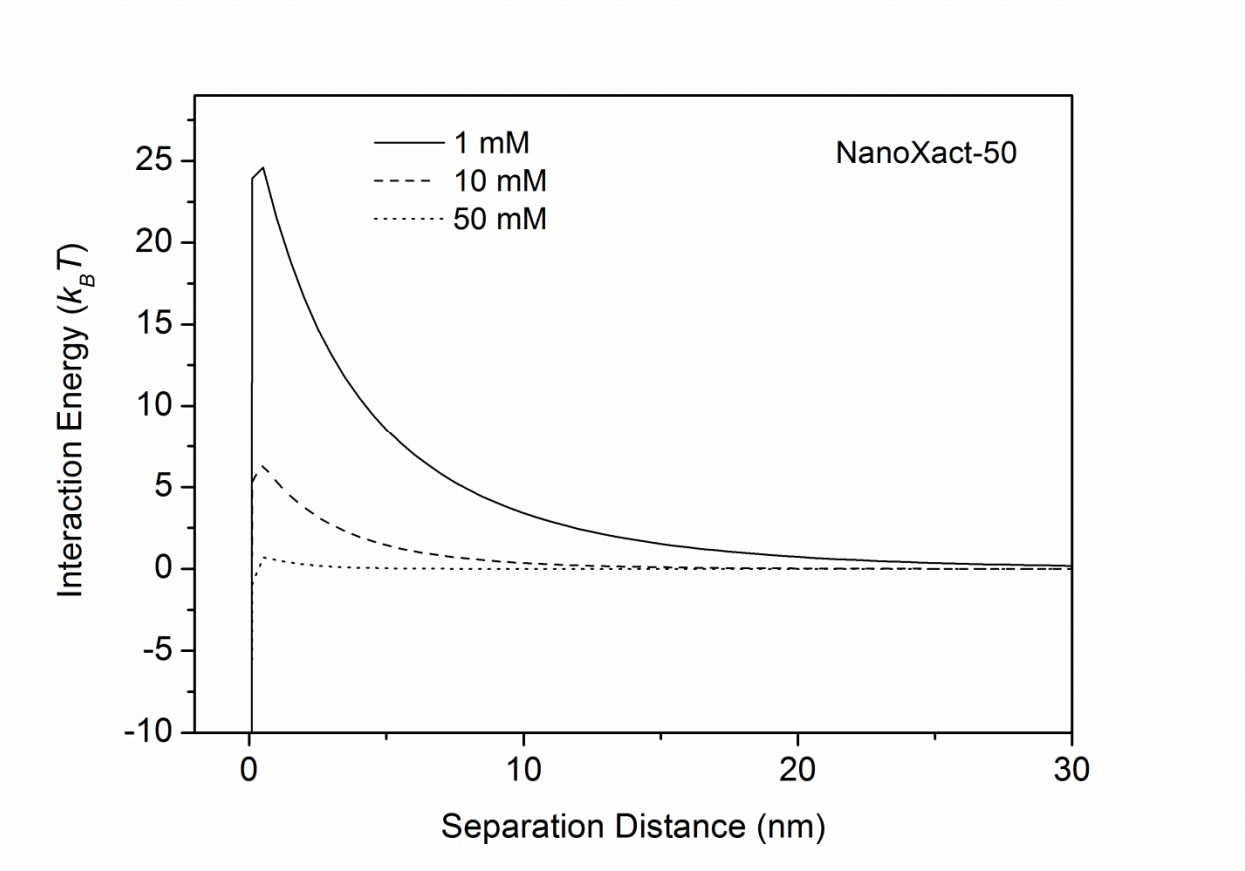

Figure S4. Interaction energy profile between NanoXact-50 nanoparticles and the ceramic collector surface as a function of separation distance for three ionic strengths.

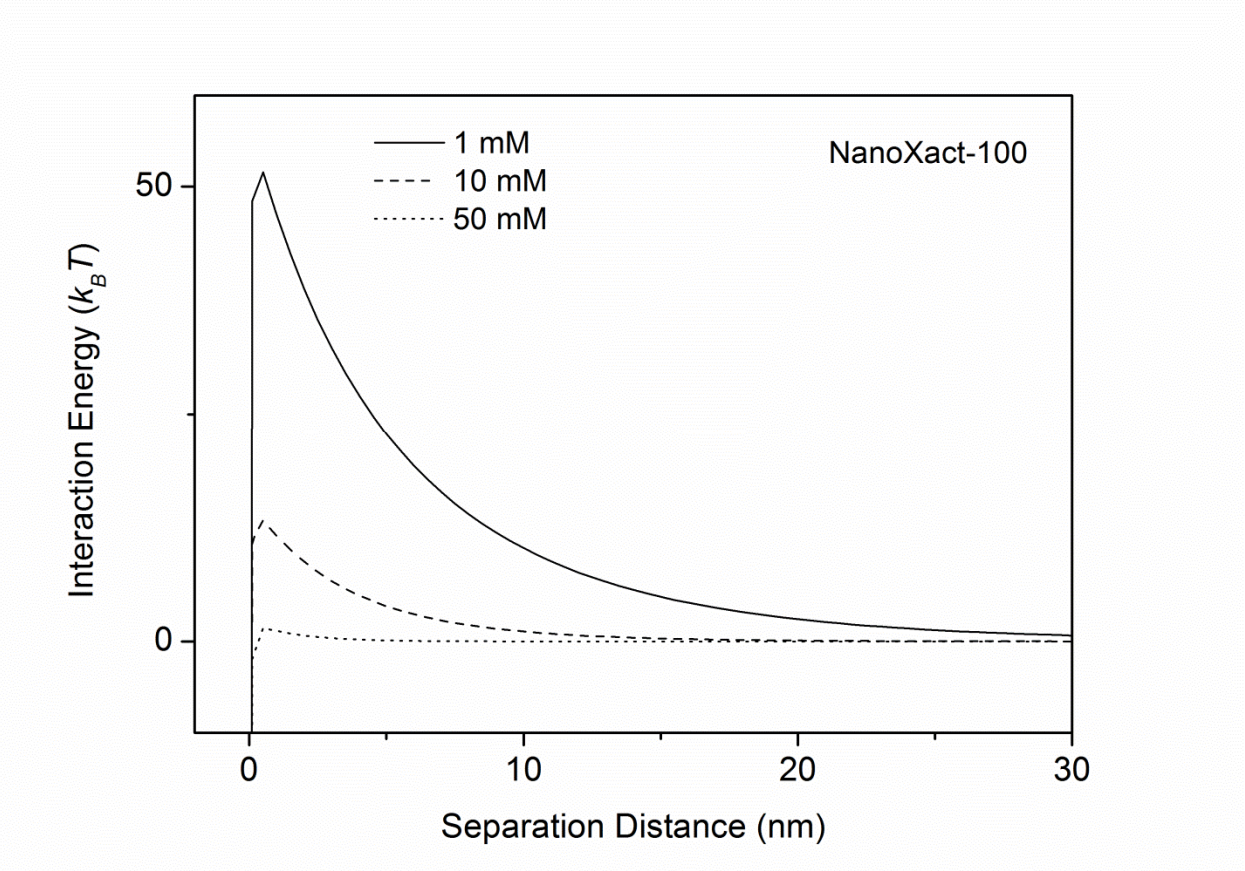

Figure S5. Interaction energy profile between NanoXact-100 nanoparticles and the ceramic collector surface as a function of separation distance for three ionic strengths.

References

1. Schijven, J. F.; Hassanizadeh, S. M.; deBruin, R., Two-site kinetic modeling of bacteriophage transport through columns of saturated dune sand. *J. Contamin. Hydrol.* **2002,** *57*, (3-4), 259-279.
2. Bradford, S. A.; Simunek, J.; Bettahar, M.; Genuchten, M. T. V.; Yates, S. R., Modeling colloid attachment, straining, and exclusion in saturated porous media. *Environ Sci Technol* **2003,** *37*, (10), 2242-2250.
3. Schijven, J. F.; Simunek, J., Kinetic modeling of virus transport at the field scale. *J. Contamin. Hydrol.* **2002,** *55*, (1-2), 113-135.
4. Elimelech, M.; Gregory, J.; Jia, X.; Williams, R. A., *Particle deposition and aggregation: Measurement, modeling, and simulation*. Butterworth-Heinemann: 1995; p 441.
5. Gregory, J., Interaction of unequal double layers at constant charge. *Journal of Colloid and Interface Science* **1975,** *51*, (1), 44-51.
6. Petosa, A. R.; Jaisi, D. P.; Quevedo, I. R.; Elimelech, M.; Tufenkji, N., Aggregation and deposition of engineered nanomaterials in aquatic environments: Role of physicochemical interactions. *Environ Sci Technol* **2010,** *44*, (17), 6532-6549.
7. Bergstrom, L., Hamaker constants of inorganic materials. *Advances in Colloid and Interface Science* **1997,** *70*, 125-169.
8. Anderson, M. T.; Lu, N., Role of microscopic physicochemical forces in large volumetric strains for clay sediments. *Journal of Engineering Mechanics* **2001,** *127*, (7), 710-719.
9. Novich, B. E.; Ring, T. A., Colloid stability of clays using photon correlation spectroscopy. *Clays Clay Miner.* **1984,** *32*, (5), 400-406.
10. Mesquita, L. M. S. d.; Lins, F. F.; Torem, M. L., Interaction of a hydrophobic bacterium strain in a hematite-quartz flotation system. *International Journal of Mineral Processing* **2003,** *71*, (1-4), 31-44.
11. Butt, H.-J.; Cappella, B.; Kappl, M., Force measurements with the atomic force microscope: Technique, interpretation and applications. *Surface Science Reports* **2005,** *59*, (1-6), 1-152.
12. Bargeman, D.; Vader, F. v. V., Van der waals forces between immersed particles. *Journal of Electroanalytical Chemistry and Interfacial Electrochemistry* **1972,** *37*, (1), 45-52.